Applied Radiation and Isotopes 166 (2020) 109434

Contents lists available at ScienceDirect

Applied Radiation and Isotopes

journal homepage: http://www.elsevier.com/locate/apradiso

Cathodoluminescence properties of La_2MoO_6:Ln^{3+} (Ln: Eu, Dy, and Sm) phosphors

M. Ayvacikli [a], Ümit H. Kaynar [b], Y. Karabulut [c], J. Garcia Guinea [d], K. Bulcar [e], N. Can [c,f,*]

[a] Manisa Celal Bayar University, Hasan Ferdi Turgutlu Technology Faculty, Mechatronics Engineering, Turgutlu-Manisa, Turkey
[b] Bakırcay University, Faculty of Engineering and Architecture, Department of Fundamental Sciences, Menemen, Izmir, Turkey
[c] Department of Physics, Manisa Celal Bayar University, Faculty of Arts and Sciences, Muradiye-Manisa, 45010, Turkey
[d] Museo Nacional Ciencias Naturales, Jose Gutierrez Abascal 2, Madrid, 28006, Spain
[e] Cukurova University, Arts-Sciences Faculty, Physics Department, 01330, Adana, Turkey
[f] Jazan University, Physics Department, P.O. Box 114, 45142, Jazan, Saudi Arabia

ARTICLE INFO

Keywords:
La_2MoO_6
Gel combustion method
XRD
Cathodoluminescience

ABSTRACT

La_2MoO_6 orange-red phosphors with high efficiency incorporated with Eu, Dy and Sm have been synthesized through a gel combustion method. The influences of rare earth doping in synthesized samples were analysed by X-ray diffraction (XRD), scanning electron microscopy-energy dispersive spectroscopy (SEM-EDS), and cathodoluminescence. Rare earth doped La_2MoO_6 samples show strong emission bands in the range of 400–750 nm and optimal doping concentration for all samples was 2 mol%. La_2MoO_6 host doped Eu ion showed intense and predominant emission peaks in 450–750 nm range. The electrical multipolar interaction contributed to the non-radiative energy transfer between Eu^{3+} ions in La_2MoO_6 host matrix. Sm doped La_2MoO_6 host exhibited orange-red CL emission peaks at 564, 608, 652 and 708 nm La_2MoO_6:Dy^{3+} phosphor displayed emissions at 484, 574 and 670 nm, respectively. The observed intense and sharp emission peaks indicate that La_2MoO_6 is promising host for lanthanides doped phosphor materials in the applications of optoelectronic.

1. Introduction

In the past two decades, trivalent lanthanides ions (Ln^{3+}) have attracted much attention as a crucial role in the development of novel phosphors due to unique properties for various applications such as agriculture, petrochemical industry, metallurgy, color display, wight light emitting diodes etc (Perhaite et al., 2017; Muresan et al., 2016; Umit et al., 2020; Coey and Sun, 1990; Binnemans et al., 2015; Haque et al., 2014). As it is known, we can achieve different emission colors (i.e. red, blue, yellow, green) from a host phosphor material by doping an appropriate Ln^{3+} ion. The color of emitted light depends on the host material and doped Ln^{3+}. For example, Eu^{3+} is a well-known activator for red phosphor (Ayvacikli et al., 2011; Halefoglu et al., 2019), Sm^{3+} for orange-red emission color (Kucuk et al., 2018), Dy for yellow and white light (Sabikoglu et al., 2012), Tb^{3+} for obtaining green light (Kaynar et al., 2020a), and Ce^{3+} for violet-blue color (Zhao et al., 2020).

It is well documented that optical properties of lanthanide ions in the host phosphor materials are strongly associated with physical and chemical properties of the matrix material itself. Therefore, it is extremely important to have a material to be used in the phosphor field. In recent years, researchers have shown an increased interest in molybdates because of their potential application in laser, phosphor, and catalysis (Meng et al., 2012; Sani et al., 2004, 2005; Kaynar et al., 2020b) but more researches are still needed.

Morphology, composition, and crystallization can influence luminescence properties of the phosphors. To date many efforts have been made to research excellent approaches for fabrication of various phosphor materials. Among them, solid state reaction method is a traditional phosphor synthesis technique that is widely used to prepare phosphor samples. However, this method requires a very long time and high reaction temperature. For instance, X. He et al. reported that Eu^{3+}-doped $La_2Mo_2O_9$ phosphor prepared by heating at 550 °C for 4 h in a furnace, followed by the calcination at 900 C for 8 h exhibited significantly enhanced red PL emission of red photoluminescence (He et al., 2011). Morphology, composition, and crystallization can influence luminescence properties of the phosphors. Therefore, a sol-gel combustion method was used instead of solid-state reaction methods in this study. As can be seen from the literature above, only Eu and Dy lanthanide ions

* Corresponding author. Department of Physics, Manisa Celal Bayar University, Faculty of Arts and Sciences, Muradiye-Manisa, 45010 Turkey.
E-mail address: ncan@jazanu.edu.sa (N. Can).

https://doi.org/10.1016/j.apradiso.2020.109434
Received 24 July 2020; Received in revised form 3 September 2020; Accepted 17 September 2020
Available online 20 September 2020

were used as an activator. Other activators should be considered to see the potential effect on the La_2MoO_6 host matrix. In addition, photoluminescence technique (PL) was used in all the studies investigated with this host material, but no work was carried out with cathodoluminescence (CL) technique.

In this study, structural and cathodoluminescence properties of La_2MoO_6 incorporated with Eu, Dy and Sm ions were collected and the details how Eu, Dy and Sm ions play roles on the host material are discussed. The motivation behind the work to be presented in this paper is due to a need for information on the results of various doped lanthanide ions because molybdates are promising candidates for luminescent host materials due to their outstanding metrics of hight stability, low photon energy and admirable intrinsic luminescence performance.

2. Experimental section

A gel combustion method has been used in order to prepare all investigated phosphor samples. Lanthanum(III) it isoxide (Merck, >99.9%), Ammonium Heptamolybdate Tetrahydrate ($(NH_4)_6Mo_7O_{24}$*$4H_2O$, Merck >99%), europium oxide (Eu_2O_3, Sigma Aldrich 99.99%), samarium oxide (Sm_2O_3, Sigma Aldrich 99.99%) and Dysprosium(III) nitrate ($Dy(NO_3)_3$, Merck >99.9%) were used as received, without further purification. Stoichiometric amounts of raw materials were weighted. In the preparation of the samples, the oxide form materials are dissolved by adding 1 M of HNO_3 and then dissolved in 10 ml of ultra pure water in a quartz beaker along with nitrates again. Citric acid ($HOC(COOH)(CH_2COOH)_2$ Merck ≥99.5) are added to this solution in the beaker and stirred with a magnetic stirrer for 1 h at 80 °C.

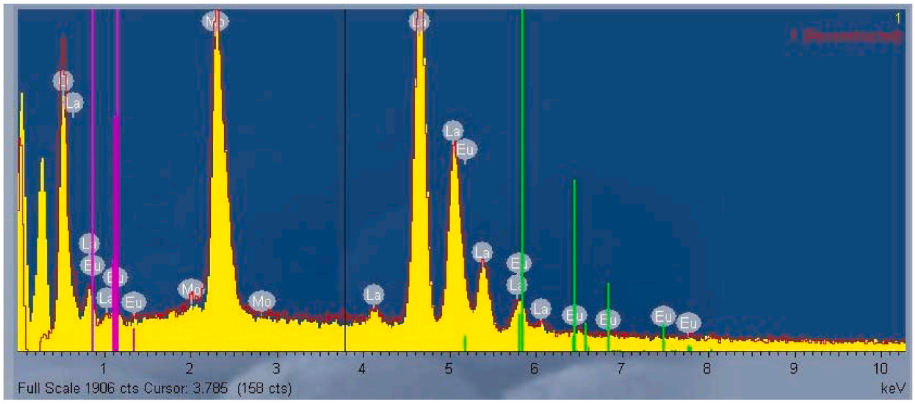

(a)

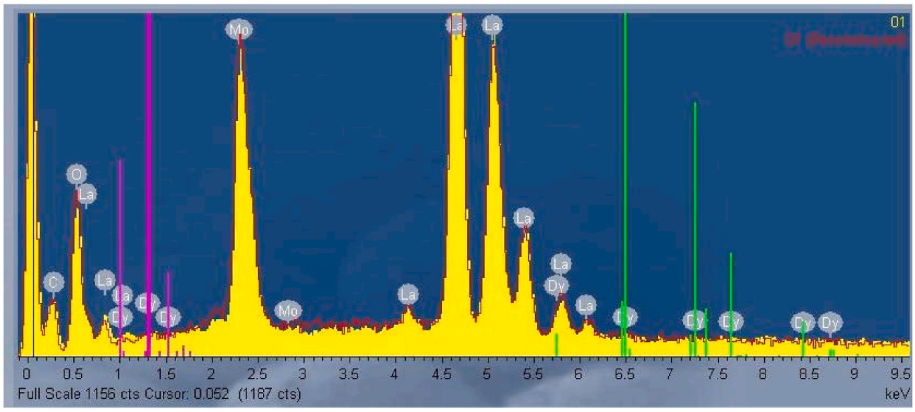

(b)

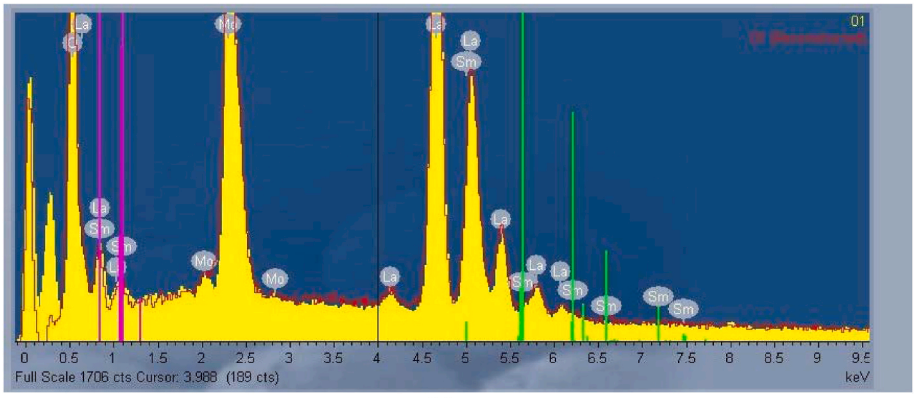

(c)

Fig. 1. EDS spectra of (a) $La_2MoO_6:Eu^{3+}$ (b) $La_2MoO_6:Dy^{3+}$ and (c) $La_2MoO_6:Sm^{3+}$.

At the end of the period, the beaker is opened, and excess water is removed at the same temperature until the gel becomes a consistency. The colorless, viscous, and consistent gel was placed in the ash oven heated at 1000 °C for 2 h. Target phosphor materials were obtained after the release of the gases with combustion reaction and used for further characterization without washing or annealing. The synthesis reaction of La_2MoO_6 sample can be described through an chemical equation such as the following.

$$42\ La(NO_3)_3{*}4H_2O + 3\ (NH_4)_6Mo_7O_{24}{*}4H_2O + 32\ HOC(CO_2H)(CH_2CO_2H)_2 \rightarrow 21\ La_2MoO_6 + 192\ CO_2\uparrow + 344\ H_2O\uparrow + 72\ N_2\uparrow$$

The investigation of phase composition of the prepared phosphor sample was carried out by a Philips PW-1710/00 diffractometer using Cu-Kα (1.5418 A) radiation at a step scan of 0.06° from 10° to 80°.The CL data were recorded in the range of 250–850 nm using a Gatan MonoCL3 detector with a PA-3 photomultiplier tube with ESEM XL30 microscope which has a chemical Energy Dispersive Spectroscopy (EDS) probe; model XLS30 of the FEI Company (2.0 A and 25 kV).

3. Results and discussion

3.1. EDS, XRD analysis and surface morphology

The Energy dispersive spectroscopy (EDS) technique was carried out at room temperature to reveal elemental compositions of involved ions in the synthesized phosphor. Several specific lines in the EDS spectra exhibit the presence of elements. EDS analysis indicates that very good agreement was observed when the concentrations of the related ions are compared to with their nominal ones (see Fig. 1). Table 1 also presents quantiles amount of the elements present in the obtained phosphors.

The phase purity and structure type of as-prepared samples were investigated by XRD analysis. Fig. 2 shows the XRD patterns of La_2MoO_6 phosphor activated with Eu^{3+}, Dy^{3+} and Sm^{3+} ions. All reflection peaks shown in the XRD patterns could be matched with a tetragonal phase La_2MoO_6 with JCPDS card number 98-002-5611 (Kaynar et al., 2020b). Unit cell parameters (i.e. a = 4.0890 Å, b = 4.0890 Å, c = 15.9900 Å, α = β = γ 90°) of La_2MoO_6 are almost identical to the standard card. The La ions in La_2MoO_6 are coordinated by eight oxygens and the Mo^{6+} ions are coordinated with four oxygen atoms. The ionic radii for the eight-coordinated La^{3+}, Eu^{3+}, Dy^{3+} and Sm^{3+} are 1.16, 1.25, 1.19 and 1.27 Å, respectively (Shannon, 1976). Due to the similar ionic radius and electric charge of trivalent rare earth (Ln^{3+}) ions, the incorporated Ln^{3+} ions prefer to substitute La sites. The strongest peak was obtained at 2θ = 27.47° which is attributed to the plane (0 1 3) for all doped samples. In the present study, the optimal Dy^{3+}, Sm^{3+}, and Eu^{3+} contents (i.e. 2 mol %) are taken into consideration which give maximum PL intensity for the samples. Therefore, the Eu_2MoO_6 phase appears in high concentrations and then the crystal structure of Eu_2MoO_6 turns from tetragonal to monoclinic. The present findings suggest that they cannot form solid solution easily at this content of Eu^{3+} ions which is consistent with the finding of previous work [13]. Similar explanation can be given for Dy^{3+} and Sm^{3+} ions. Although many attempts, including variation of composition and sintering temperature or time, it appears that the addition of Sm^{3+}, Dy^{3+} and Eu^{3+} leads to a small amount of impurity phases in the XRD pattern but those will not give rise to any negative effect on CL spectrum. This confirms that doped ions were effectively incorporated into the host matrix

Table 1
Quantitative analysis of elemental analysis of La_2MoO_6 doped with (a) Eu^{3+}, (b) Dy^{3+} and (c) Sm^{3+} by EDS spectra.

Element	Weight%	Atomic%
O	21.15	67.34
Mo	23.05	12.24
La	54.12	19.85
Eu	1.68	0.56
Element	Weight%	Atomic%
O	21.01	67.22
Mo	22.56	12.04
La	55.42	20.42
Dy	1.01	0.32
Element	Weight%	Atomic%
O	21.18	67.38
Mo	23.18	12.29
La	53.91	19.75
Sm	1.73	0.59

The crystallite size was assessed from a single diffraction peak using the Scherrer's equation

$$D = \frac{k\lambda}{\beta cos\theta}$$

where λ is the x-ray wavelength, β is the full width at half maximum (FWHM) of the peak at a selected angle, D is the crystallite size of the scattering particles in nm. Crystallite sizes are calculated for Eu, Dy and Sm incorporated La_2MoO_6 phosphor samples at selected 3 dominant diffraction planes, i.e. (0 1 3), (1 1 6) and (1 2 3). The respective average size of resulting nanoparticles of La_2MoO_6:Eu^{3+} and La_2MoO_6:Dy^{3+} and La_2MoO_6:Sm^{3+} are estimated to about 39.61 nm, 57.49 nm, and 45.12 nm.

SEM images of La_2MoO_6:Eu^{3+}, La_2MoO_6:Dy^{3+} and La_2MoO_6:Sm^{3+} are shown inFig. 3 From these images, the phosphor samples demonstrate obvious agglomeration and irregular shape with some porous structure. It is noted that the morphology of the samples did not significantly change when the dopant type changes.

3.2. Cathodoluminescence spectra of Ln^{3+} doped La_2MoO_6 phosphor

Cathodoluminescence (CL) is the emission of photons of characteristics wavelengths from a material which is excited with a beam of electrons and analogous to the photoluminescence process. The CL emission spectra of the host phosphor activated with Sm, Eu and Dy ions were analysed using the highly sensitive photomultiplier. Our findings showed that the maximum CL emission intensity of Sm^{3+}, Dy^{3+} and Eu^{3+} activated samples synthesized using a wet chemical method were observed when Sm^{3+}, Dy^{3+} and Eu^{3+} amounts reached 2 mol%.

The CL data were collected in the range of 250–850 nm. It should be stressed that at the lower acceleration voltage, the main characteristic emission lines of Eu^{3+} were not observed. The emission peaks started to appear when the accelerating voltage was increased. This suggests that many activators ions inside of the particles were excited due to the deeper penetration of electrons. Fig. 4 depicts the CL emission spectrum of La_2MoO_6 doped with Eu ion under excitation of the low voltage electron beam excitation (7 keV) and filament current 55 μA. As seen from data, the CL emission spectral profiles mostly consisted of a series of narrow and intense emission lines corresponding to the $^5D_0 \rightarrow {}^7F_J$ transitions of Eu^{3+} ions. However, observed emission lines can be divided seven transition groups; (i) 534 nm ($^5D_1 \rightarrow {}^7F_1$) (ii) 554 nm ($^5D_1 \rightarrow {}^7F_2$), (iii) 580 nm,588 nm, and 594 nm ($^5D_0 \rightarrow {}^7F_1$), (iv) 614 nm and 622 nm ($^5D_0 \rightarrow {}^7F_2$), (v) 656 nm ($^5D_0 \rightarrow {}^7F_3$), (vi) 696 nm ($^5D_0 \rightarrow {}^7F_4$) and (vii) 706 nm ($^5D_0 \rightarrow {}^7F_5$). The energy level diagram next to Fig. 4 explains how the emission process occurs from $^5D_1$ and $^5D_0$ excited state of Eu^{3+} ions to other states aforementioned. It is clearly apparent that the intensity of each transition is different from each other. Among the emission lines, the predominant one is $^5D_0 \rightarrow {}^7F_2$ transition centred at 614 and 622 nm and those emission lines give rise to red light emission. As expected, when Eu^{3+} ions occupy a site with inversion symmetry, only the magnetic dipole (MD) transition should be allowed according to Judd-Ofelt theory. Whereas both electric and magnetic dipole transitions are allowed which indicates that Eu^{3+} occupies a non-centrosymmetric environment. The $^5D_0 \rightarrow {}^7F_2$ transition (i.e. 614 and 622), being a hypersensitive electric dipole transition is significantly

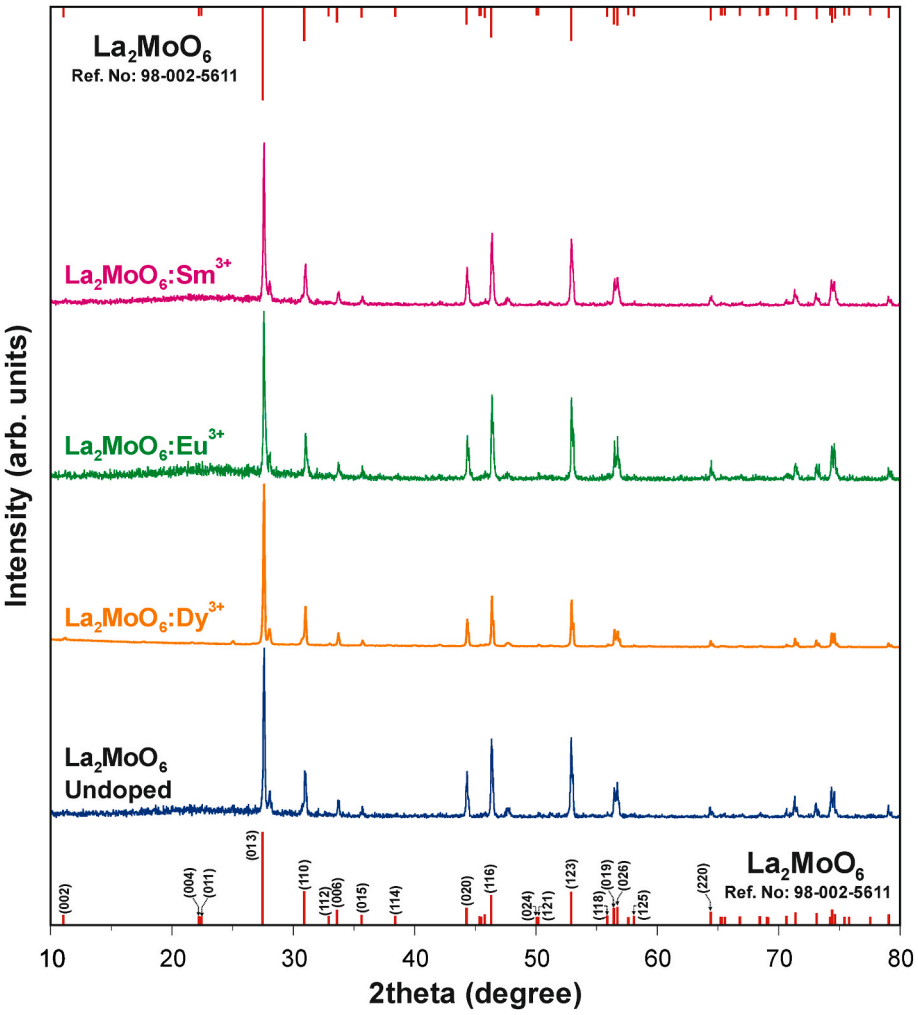

Fig. 2. XRD patterns of La_2MoO_6 and La_2MoO_6:La^{3+} (La: Eu^{3+}, Sm^{3+} and Dy^{3+}).

affected by the chemical environment around Eu^{3+} ions, whereas the magnetic dipole allowed $^5D_0 \rightarrow {}^7F_1$ transition is insensitive to changes in the chemical environment (Ayvacikli et al., 2011; Boronat et al., 2017). In our case, electric dipole transition is dominant compared to magnetic dipole transition with the selection rule $\Delta J = 0, \pm 1$ and it indicates that the Eu^{3+} ion is located at the non-inversion symmetric sites in the La_2MoO_6 lattice (Patel et al., 2013). In other words, electric dipole transition plays a leading role in this lattice.

Fig. 5 shows emission spectrum of Sm^{3+} doped La_2MoO_6 phosphors under electron beam excitation. As seen from the data, all emission spectrum from 500 to 750 nm are composed of four dominating yellow-orange-red emission peaks located at 564–576 nm, 608 nm, 652–666 nm and 708 nm, which are assigned to $^4G_{5/2} \rightarrow {}^6H_{5/2}$, $^4G_{5/2} \rightarrow {}^6H_{7/2}$, $^4G_{5/2} \rightarrow {}^6H_{9/2}$, and $^4G_{5/2} \rightarrow {}^6H_{11/2}$ transitions of Sm^{3+} ions, respectively (Kucuk et al., 2018; Hou et al., 2020). The first emission peaks centred at 564 and 576 nm (yellow) corresponding to $^4G_{5/2} \rightarrow {}^6H_{5/2}$ is a magnetic-dipole (MD) moment transition, the second emission peak located at 608 nm ($^4G_{5/2} \rightarrow {}^6H_{7/2}$) is due to partially magnetic and electrical dipole moments based on the selection rule $\Delta J = \pm 1$, the third transition ($^4G_{5/2} \rightarrow {}^6H_{9/2}$) located at 652 and 666 nm is due to purely electric dipole moment according to the selection rule of $\Delta J = 2$ (Yu et al., 2014). From the data in Fig. 5, it is apparent that the emission intensity at 608 nm is more dominant compared to other emission lines. The intensity ratio between 608 nm (ED) and 564–576 nm (MD) is a measure for the variation symmetry, coordination and distortion around Sm^{3+} environment. This indicates La_2MoO_6 shows asymmetrical behaviour.

As for Dy^{3+} doped La_2MoO_6 phosphor, the CL emission peaks were collected, and two intense emission peaks were observed: one at 484 and 494 nm (blue) and the other at 574 nm (yellow) as seen from Fig. 6. In addition, one low intensity peak is also seen in the emission spectrum at 670 nm. The two strong peaks located at 484–494 nm and 574 nm are attributed to $^4F_{9/2} \rightarrow {}^6H_{15/2}$, $^4F_{9/2} \rightarrow {}^6H_{13/2}$, respectively. One low intensity peak at 670 nm is assigned to $^4F_{9/2} \rightarrow {}^6H_{11/2}$ (Wani et al., 2015). The $^4F_{9/2} \rightarrow {}^6H_{13/2}$ transition is assigned to the hypersensitive transition whilst $^4F_{9/2} \rightarrow {}^6H_{15/2}$ belongs to magnetic dipole transition of Dy^{3+} ion in La_2MoO_6 environment. It is quite familiar that the hypersensitive transition $^4F_{9/2} \rightarrow {}^6H_{13/2}$ ($\Delta L = 2$, $\Delta J = 2$) is extremely affected by the surrounding environment and is assigned to the forced electric dipole (FED) transition. The transition $^4F_{9/2} \rightarrow {}^6H_{15/2}$ ($\Delta L = 2$, $\Delta J = 3$) centred at 484–494 nm corresponds to the magnetic dipole (MD) transition and it is unsusceptible to the surrounding environment around the Dy^{3+} ions (Dai et al., 2020). Dy^{3+} ion is placed in the La_2MoO_6 host material in two different ways: a low symmetry local site and a hight symmetry local site. In the low symmetry local site (i.e. without inversion symmetry) yellow emission is often dominant in the CL emission spectrum whereas in the high symmetry local site (i.e inversion symmetry center) the blue emission peak is stronger than that of the yellow emission. In our case, the former one takes place for Dy^{3+} incorporated La_2MoO_6 phosphor.

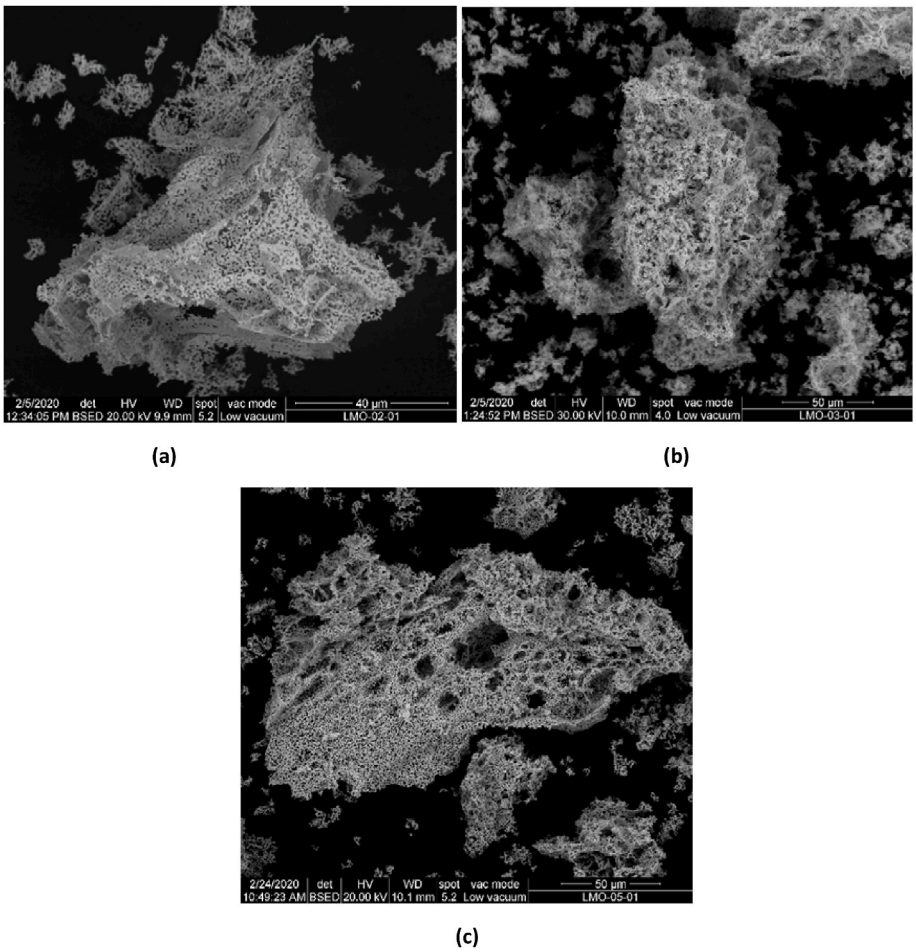

Fig. 3. ESEM images of (a) $La_2MoO_6:Eu^{3+}$ (b) $La_2MoO_6:Dy^{3+}$ and (c) $La_2MoO_6:Sm^{3+}$ prepared by a gel combustion method.

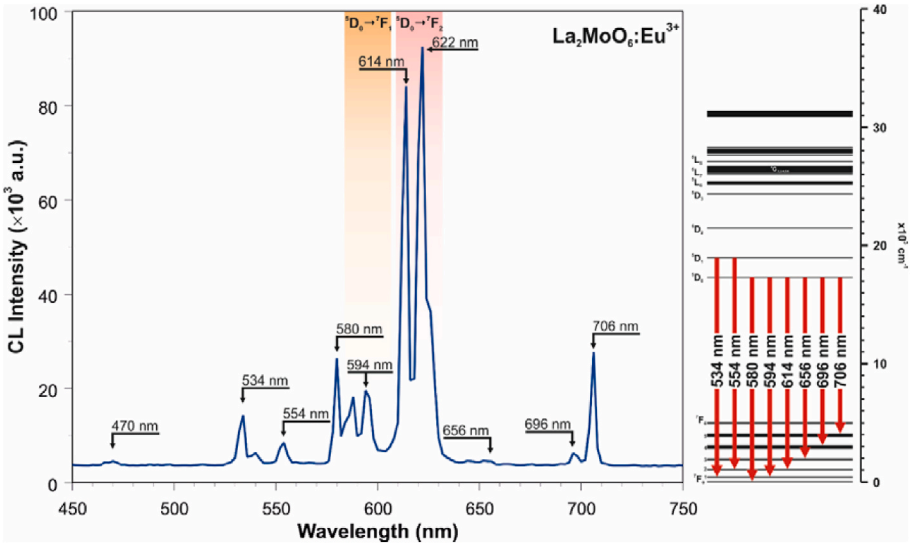

Fig. 4. The CL emission spectrum of the tetragonal phased La_2MoO_6phosphor doped with Eu^{3+} ion under 25 kV accelerating voltage.

4. Conclusions

Eu, Dy and Sm doped La_2MoO_6 phosphors have been prepared via a gel combustion method. The crystal structure was carried out by XRD technique and prepared samples presented tetragonal phase. EDS were introduced to analyse La_2MoO_6 doped with Eu, Sm and Dy ions. Characteristic emission for Eu is obtained with maxima at 614 and 622 nm corresponding to $^5D_0 \rightarrow {}^7F_2$ transition (ED). In the present case, typical f-f transitions of Eu ion are observed. Non-radiative energy transfer of Eu^{3+} ions was induced by electrical multipolar interaction. Emission peaks at 484 nm and 494 nm are due to the magnetic dipole $^4F_{9/2} \rightarrow {}^6H_{15/2}$ transition and peak at 574 nm is due electric dipole $^4F_{9/2}$

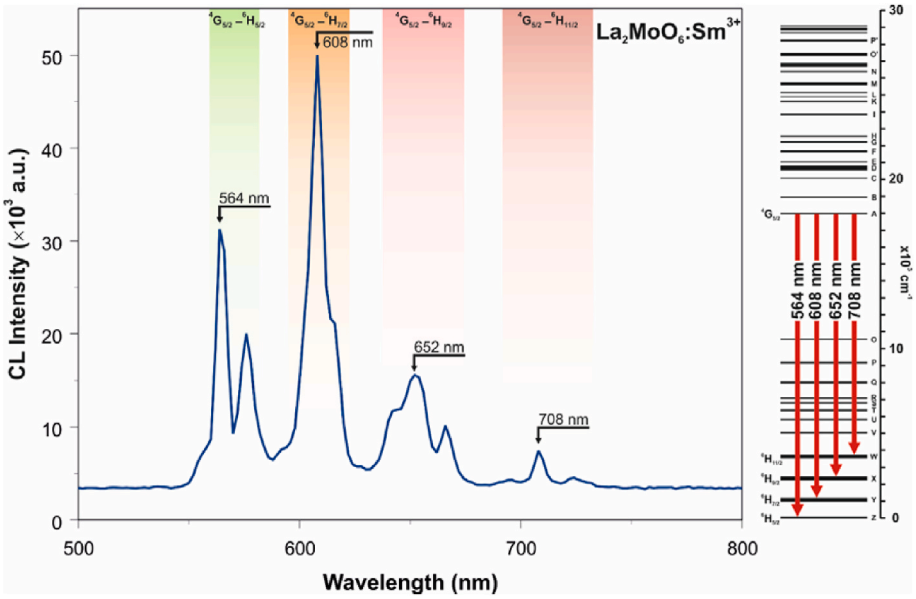

Fig. 5. The CL emission spectrum of the tetragonal phased La_2MoO_6 phosphor doped with Sm^{3+} ion under 25 kV accelerating voltage.

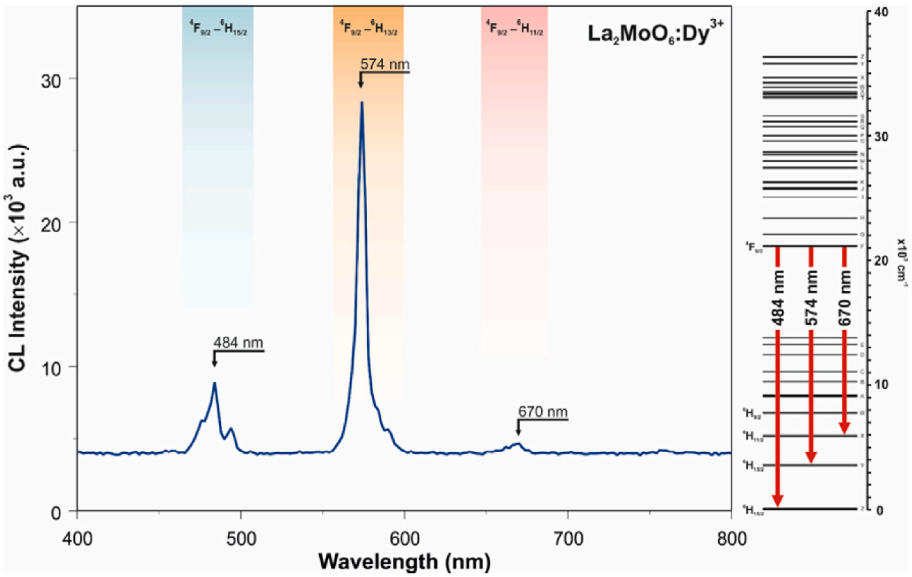

Fig. 6. The CL emission spectrum of the tetragonal phased La_2MoO_6 phosphor doped with Dy^{3+} ion under 25 kV accelerating voltage.

→ $^6H_{13/2}$ transition of Dy^{3+} ions. $La_2MoO_6:Sm^{3+}$ sample exhibited four luminescence peaks appeared at 564 nm, 608 nm, 652 nm and 708 nm, showing an orange-red emission. Further investigations are in progress to elucidate the influence of other lanthanides ions in La_2MoO_6 host as a co-activator in optoelectronic applications.

Declaration of competing interest

The authors declare that they have no known competing financial interests or personal relationships that could have appeared to influence the work reported in this paper.

References

Ayvacikli, M., Ege, A., Yerci, S., Can, N., 2011. Synthesis and optical properties of Er^{3+} and Eu^{3+} doped $SrAl_2O_4$ phophor ceramic. J. Lumin. 131, 2432–2439.

Binnemans, K., Jones, P.T., Blanpain, B., Gerven, T.V., Pontikes, Y., 2015. Towards zero-waste valorisation of rare-earth containing industrial process residues: a critical review. J. Clean. Prod. 99, 17–38.

Boronat, C., Rivera, T., Garcia Guinea, J., Correcher, V., 2017. Cathodoluminescence emission of REE (Dy, Pr and Eu) doped $LaAlO_3$ phosphors. Radiat. Phys. Chem. 130, 236–242.

Coey, J.M.D., Sun, H., 1990. Improved magnetic properties by treatment of iron-based rare earth intermetallic compounds in anmonia. J. Magn. Magn Mater. 87, 251–254.

Dai, T., Ju, G., Jin, Y., Zhou, X., Li, Y., Wu, H., Hu, Z., Hu, Y., 2020. Novel yellow color-emitting $BaY2O4:Dy^{3+}$ phosphors: persistent luminescence from blue to red. Appl. Phys. A 126, 217.

Halefoglu, Y.Z., Oglakci, M., Yuksel, M., Canimoglu, A., Topaksu, M., Can, N., 2019. Structural and spectroscopic properties of $LaAlBO_3$ doped with Eu^{3+} ions. Appl. Radiat. Isot. 154, 108876.

Haque, H., Hughes, A., Lim, S., Vernon, C., 2014. Rare earth elements: overview of mining, mineralogy, uses, sustainability and environmental impact. Resources 3, 614–635.

He, X., Guan, M., Zhang, C., Shnag, T., Lian, N., Zhou, Q., 2011. Luminescence enhancement of Eu^{3+} activated $La_2Mo_2O_9$ red-emitting phosphor through chemical substitution. J. Mater. Res. 26, 2379–2383.

Hou, Y., Chen, W., Xia, J., Liu, B., Peng, L., Wang, J., Qiang, Q., 2020. Synthesis and luminescence characteristic of whitlockite-type $AgCa_{10}(PO_4)_7:RE^{3+}$ (RE=Sm,Dy) phosphors. Optic Laser. Technol. 125, 106042.

Kaynar, Umit H., Cam Kaynar, S., Ayvacikli, M., Karabulut, Y., Souadi, G.O., Can, N., 2020a. Influence of laser excitation power on temperature-dependent luminescence behaviour of Ce- and Tb-incorporated $BaMgAl_{10}O_{17}$ phosphors. Radiat. Phys. Chem. 168, 108617.

Kaynar, U.H., Cam Kaynar, S., Alajlani, Y., Ayvacikli, M., Karali, E., Karabulut, Y., Akca, S., Karali, T., Can, N., 2020b. Eu3+ and Dy^{3+} doped La_2MoO_6 and $La_2Mo_2O_9$ phosphors: synthesis and luminescence properties. Mater. Res. Bull. 123, 110723.

Kucuk, N., Bulcar, K., Dogan, T., Garcia Guinea, J., Portakal, Z.G., Karabulut, Y., Ayvacikli, M., Canimoglu, A., Topaksu, M., Can, N., 2018. Doping Sm^{3+} into ZnB_2O_4 phosphors and their structural and cathodoluminescence properties. J. Alloys Compd. 748, 245–251.

Meng, F., Zhang, X., Li, H., Jin Seo, H., 2012. Synthesis and spectral characteristics of $La_2MoO_6:Ln^{3+}$ (Ln=Eu, Sm, Dy, Pr, Tb) polycrystals. J. Rare Earths 30, 866–870.

Muresan, L.E., Karabulut, Y., Cadis, A.I., Parhaita, I., Canimoglu, A., Garcia Guinea, J., Barbu Tudoran, L., Silipas, D., Ayvacikli, M., Can, N., 2016. Tunable luminescence of broadband-excited and narrow line green emitting $Y_2SiO_5:Ce^{3+},Tb^{3+}$ phosphor. J. Alloys Compd. 658, 356–366.

Patel, D.K., Vishwanadh, B., Sudarsan, V., Kulsreshtha, S.K., 2013. Difference in the nature of Eu3+ environment in Eu3+ doped BaTiO3 and BaSnO3. J. Am. Ceram. Soc. (96), 3857–3861.

Perhaite, I., Muresan, L.E., Silipas, D.T., Borodi, G., Karabulut, Y., Garcia Guinea, J., Ayvacikli, M., Can, N., 2017. The role of calcination temperature on structural and luminescence behaviour of novel apatite-based $Ca_2Y_8(SiO_4)_6O_2:Ce^{3+}$, Tb^{3+} phosphors. Appl. Radiat. Isot. 130, 188–197.

Sabikoglu, I., Ayvacikli, M., Bergeron, A., Ege, A., Can, N., 2012. Photoluminescence investigations of Li_2SiO_3:Ln (Ln=Er^{3+}, Eu^{3+}, Dy^{3+}, Sm^{3+}). J. Lumin. 132, 1597–1602.

Sani, D. MaE., Toncerrero-Lopez, A., Nunez, P., Abril, M., Lavin, V., Rodriguez-Mendoza, U.R., Rodriguez, V.D., 2004. Synthesis, electrical properties, amd optical characterization of Eu^{3+} doped $La_2Mo_2O_9$ nanocrystalline phosphors. J. Non-Cryst. Solids 345–346, 377.

Sani, E., Toncelli, A., Tonelli, M., Lis, D.A., Zharikov, E.V., Subbotin, K.A., Smirnov, V.A., 2005. Effect of cerium cooping in Er^{3+},Ce^{3+}:$NaLa(MoO_4)_2$ crystals. J.App. Phys. 97, 123531, 1.

Shannon, R.D., 1976. Revised, effective ionic radii and systematic studies of interatomic distances in halides and chalcogenides. Acta Crystallogr. 32, 751–767.

Umit, H., Kaynar, S., Kaynar, Cam, Ayvacikli, M., Karabulut, Y., Souadi, G.O., Can, N., 2020. Influence of laser excitation power on temperature dependent luminescence behaviour of Ce-and Tb-incorporated $BaMgAl_{10}O_{17}$ phosphors. Radiat. Phys. Chem. 168, 108617.

Wani, J.A., Dhoble, N.S., Lochab, S.P., Dhoble, S.J., 2015. Luminescence characteristics of C^{5+} ions and ^{60}Co irradiated $Li_2BaP_2O_7:Dy^{3+}$ phosphor. Nucl. Instrum. Methods B 349, 56–63.

Yu, R., Mi Noh, H., Kee Moon, B., Chun Choi, B., Hyun Jeong, J., Sueb Lee, H., Jang, K., Soo Yi, S., 2014. Photoluminescence characteristics of Sm^{3+} doped $Ba_3La(PO_4)$ as new orange-red emitting phosphors. J. Lumin. 145, 717–722.

Zhao, Y., Wang, S., Han, Y.J., Zhang, J.Y., Liu, C., Hu, X.F., Zhang, Z.W., Wang, L.J., 2020. Luminescence properties and energy transfer in Ce^{3+} and Tb^{3+} co-doped $Sr_5(PO_4)_2SiO_4$ phosphor. J. Lumin. 223, 117253.